A position-based PFEM formulation for free-surface non-Newtonian flows with application to fresh concrete

Luiz Fernando Honorato Teodoro[1], Giovane Avancini[2], Rodolfo André Kuche Sanches[1]

[1]*Structural Engineering Department, São Carlos School of Engineering, University of São Paulo*
Av. Trabalhador Saocarlense, 400, São Carlos, São Paulo, Brazil
luizteodoro@usp.br, rodolfo.sanches@usp.br
[2]*Structural Engineering Department, School of Civil Engineering, Architecture, and Urbanism, State University of Campinas*
Av. Albert Einstein, 951, Campinas, São Paulo, Brazil
giovanea@unicamp.br

Abstract. This work presents a methodology for free surface non-Newtonian incompressible flows using a particle position-based formulation of the Particle Finite Element Method (PFEM), motivated by the simulation of fresh concrete flow. This method is based on the Lagrangian description of the flow and represents the fluid domain by cloud of particles, with a finite element mesh being built, taking the particles as nodes, to solve the motion equations and update the particle positions. To deal with large distortions of fluid flows, such mesh is constantly rebuilt, leading to a method very robust to deal with topological changes within the fluid domain. This approach requires updating the reference configuration, enabling the use of partially or fully updated Lagrangian descriptions. The weak solution is based on the stationary energy principle considering current nodal positions and pressures as variational parameters, deviating from the common practice of employing velocity and pressure as unknowns. Furthermore, smoothed version of the Bingham viscoplastic model is chosen to represent the fresh concrete behavior, keeping stresses independent of strain history and making updating the reference for the fluid simple, without the need for considering the stress distribution in the past reference. The implicit α-generalized strategy is chosen for time integration, enabling second order convergence and ensuring good stability due to the control over numerical dissipation at high frequencies. Finally, selected 3D example is simulated to test and verify the proposed methodology.

Keywords: PFEM; non-Newtonian; concrete flow.

1 Introduction

The computational simulation of flows with moving boundaries, particularly free surfaces flows with topological changes, presents a significant challenge. In this context, the methodologies can be divided into two main classes: mesh-based methods and particle methods, also known as meshless methods. These methodologies can be described using Eulerian (spatial), Arbitrary Lagrangian-Eulerian (ALE) or Lagrangian (material) approaches.

In the Eulerian description, fluid properties are recorded at fixed points in space on a fixed mesh, referencing the current configuration. When using this approach to simulate such flows, besides selecting methods to solve the governing equations (e.g., FEM, FDM, FVM), additional techniques are needed to track the free surface movement. Techniques like Marker and Cell (MAC), Simple Line Interface Calculation (SLIC), Volume of Fluid (VoF), and Level Set methods were introduced by Welch et al. [1], Noh and Woodward [2], Hirt and Nichols [3], and Osher and Sethian [4], respectively.

Hirt et al. [5] proposed the ALE method in the context of finite differences, enabling independent mesh motion from the fluid, then facilitating the solution of various free surface problems. However, despite the mesh's ability to move, it still struggles with topological changes due to severe distortions compromising simulation stability.

In the Lagrangian approach, material properties are tracked along the trajectory of each particle, using the initial configuration as a reference. Within the context of mesh-based methods, the Lagrangian description can be used to simulate free surface flows by restricting displacements and strains to finite values. This is done to avoid large mesh distortions that compromise simulation stability (see e.g. in Avancini and Sanches [6]). However, this limitation restricts the scope to a small set of problems.

Within the realm of particle methods, several techniques stand out for their ability to handle flows with free surfaces and topological changes, adopting Lagrangian description. These include the Discrete Element Method (DEM) proposed by Cundall and Strack [7], Smoothed Particle Hydrodynamics (SPH) developed by Gingold and Monaghan [8], and the Moving Particle Semi-implicit (MPS) method introduced by Koshizuka and Oka [9].

To integrate the precision and robustness of mesh-based techniques with the advantages of particle-based methods, Idelsohn et al. [10] introduced a novel hybrid approach known as the Particle Finite Element Method (PFEM). This procedure integrates periodic remeshing with the α-shape method to delineate fluid boundaries. Cremonesi et al. [11] provides a good overview of the theory and applications of PFEM, highlighting its potential to simulate free surface flows, fluid-structure interaction, industrial processes, and landslide flows.

Additionally, Coda [12], inspired by the work of Bonet et al. [13], proposed a FEM formulation for large deformation problems where the unknown variables are the nodal positions instead of displacements. This naturally incorporates geometric nonlinearities into the formulation. Based on this method, Avancini et al. [14] proposes a particle-position-based PFEM approach for incompressible Newtonian flows. Such method eliminates the need for an additional step to compute displacements from particle velocities, naturally incorporates geometric nonlinearities via the deformation gradient, and is well-suited for monolithic simulation of fluid-structure interaction (FSI) problems, aligning with the typical representation of hyperelastic materials in terms of position or displacement.

This work extends the application of the particle-position-based PFEM formulation to incompressible non-Newtonian fluids, seeking application to fresh concrete flow modeling. It is also based on previous works by Reinold et al. [15], Reinold and Meschke [16], Franci and Zhang [17] and Cremonesi et al. [18], that simulated fresh concrete flows using conventional PFEM.

Newtonian fluids are characterized by constant dynamic viscosity, with linear relation of shear stress with distortion rate. However, for non-Newtonian fluids, this parameter varies with the strain rate according to the appropriate curve modeling the specific fluid. Specifically for the flow of fresh cement-based materials, such as mortar and concrete in their fresh state, two approaches are commonly used to model the material behavior: viscoplastic and elasto-viscoplastic models.

The viscoplastic models include the Bingham model, adopted by Reinold et al. [15], Li et al. [19], Tran-Duc et al. [20], Franci and Zhang [17], Abo Dhaheer et al. [21], Lashkarbolouk et al. [22], and Cremonesi et al. [18], and the Herschel-Bulkley model, adopted by Jiang et al. [23], Mu et al. [24], Li et al. [19], and Feys et al. [25]. Moreover, the elasto-viscoplastic models are adopted in the studies of Reinold and Meschke [16], and Hosseinpoor et al. [26], showing that elasto-viscoplastic models can simulate the behavior of fresh concrete more accurately.

In this work, we chose the Bingham viscoplastic model due to its simplicity of implementation and lower computational cost. It keeps stresses independent of strain history and simplify updating the reference for the fluid without needing to consider past stress distribution. Moreover, it provides satisfactory results for most applications.

2 Governing equations

In the following sections, we provide a brief discussion of the most relevant aspects of the particle-position-based PFEM. More details about this formulation are given in Avancini et al. [14]. This uses a partially updated Lagrangian description, taking the previous time step equilibrium configuration of the continuum as reference. Let Ω_r be the fluid domain in the reference configuration at instant $t_n < t_{n+1}$. Where the subscript r refers to reference configuration. The reference and current configurations are defined by the coordinates $\mathbf{x}_r$ and $\mathbf{y}$, respectively. The deformation gradient tensor $\mathbf{F}_r$ is then defined as:

$$\mathbf{F}_r = \nabla_{\mathbf{x}_r} \mathbf{y} \tag{1}$$

The governing equations are the momentum and mass conservation, with the latter can be expressed in terms of the Jacobian determinant ($J_r = |\mathbf{F}_r|$), which represents the volumetric change of an infinitesimal element relative to its reference volume. Under the assumption of fully incompressible flow, the Jacobian equals one. Therefore, these equations in the reference configuration can be written as:

$$\rho \ddot{\mathbf{y}} - \nabla_{\mathbf{x}_r} \cdot \left(\mathbf{S} \mathbf{F}_r^T \right) - \mathbf{b}_r = \mathbf{0} \tag{2}$$

$$J_r - 1 = 0 \tag{3}$$

where ρ is the fluid density, $\ddot{\mathbf{y}}$ is the material derivative of fluid velocity, $\mathbf{S}$ is the second Piola-Kirchhoff stress tensor, and $\mathbf{b}_r$ is the body force vector.

The governing equations are complemented by the boundary conditions, expressed as:

$$\mathbf{y} = \mathbf{y}_D \text{ on } \Gamma_D \tag{4}$$

$$\left(\mathbf{S}\mathbf{F}_r^T\right)\mathbf{n}_r = \mathbf{h}_r \text{ on } \Gamma_N \tag{5}$$

where $\mathbf{y}_D$ are the positions prescribed at the Dirichlet boundary (Γ_D), $\mathbf{h}_r$ are the tractions precribed at the Neumann boundary (Γ_N), and $\mathbf{n}_r$ is the normal vector to Γ_N.

2.1 Constitutive law

The Cauchy stress, defined in the current configuration Ω, is given by:

$$\boldsymbol{\sigma} = \boldsymbol{\tau} - p\mathbf{I} \tag{6}$$

where $\boldsymbol{\tau}$ is the deviatoric stress tensor, p is the pressure, and $\mathbf{I}$ is the identity tensor.

Following Bingham model, the deviatoric stress tensor is given by:

$$\boldsymbol{\tau} = 2\widetilde{\mu}\dot{\boldsymbol{\varepsilon}} = 2\left(\mu_p + \frac{\tau_0}{\|\dot{\boldsymbol{\varepsilon}}\|}\right)\dot{\boldsymbol{\varepsilon}} \qquad \text{if} \qquad \|\dot{\boldsymbol{\varepsilon}}\| \neq 0 \tag{7}$$

$$\|\boldsymbol{\tau}\| \leq \tau_0 \qquad \text{if} \qquad \|\dot{\boldsymbol{\varepsilon}}\| = 0 \tag{8}$$

where $\widetilde{\mu}$ is the apparent viscosity, μ_p is the plastic viscosity, τ_0 is the yield stress and $\|\dot{\boldsymbol{\varepsilon}}\|$ is the equivalent strain rate which is calculated as follows:

$$\|\dot{\boldsymbol{\varepsilon}}\| = \sqrt{2\dot{\boldsymbol{\varepsilon}} : \dot{\boldsymbol{\varepsilon}}} \tag{9}$$

and the strain rate tensor is given by:

$$\dot{\boldsymbol{\varepsilon}} = \frac{1}{2}\left(\nabla_{\mathbf{y}}^T\dot{\mathbf{y}} + \nabla_{\mathbf{y}}\dot{\mathbf{y}}\right) \tag{10}$$

where $\dot{\mathbf{y}}$ is the velocity vector.

When the equivalent strain rate tends to zero, from eq. (7), the apparent viscosity tends to infinity, which induces numerical difficulties. To avoid this, regularization techniques, such as the one proposed by Papanastasiou [27] and adopted in the present work, that regularize the constitutive law yielding a single expression:

$$\boldsymbol{\tau} = 2\left(\mu_p + \frac{\tau_0}{\|\dot{\boldsymbol{\varepsilon}}\|}\left(1 - e^{-m\|\dot{\boldsymbol{\varepsilon}}\|}\right)\right)\dot{\boldsymbol{\varepsilon}} \tag{11}$$

where m is a regularization parameter. The higher m value, the better it approximates the original Bingham model; in this present work, it is set to 1000.

The deviatoric stress tensor can be written as the double contraction between an Eulerian constitutive tensor and the Eulerian strain rate tensor as:

$$\boldsymbol{\tau} = \boldsymbol{\mathcal{D}} : \dot{\boldsymbol{\varepsilon}} \tag{12}$$

with $\boldsymbol{\mathcal{D}}$ being a 4th order consitutive of components:

$$\boldsymbol{\mathcal{D}}_{ijkl} = \left(\mu_p + \frac{\tau_0}{\|\dot{\boldsymbol{\varepsilon}}\|}\left(1 - e^{-m\|\dot{\boldsymbol{\varepsilon}}\|}\right)\right)\left(\delta_{ik}\delta_{jl} + \delta_{il}\delta_{jk}\right), \tag{13}$$

with δ denoting the Kronecker delta.

Since the formulation occurs in the reference configuration, which is the last state of equilibrium, the constitutive law needs to be expressed in this reference. Consequently, we use the second Piola-Kirchhoff stress tensor and the Green-Lagrange strain rate tensor, which are defined as follows, respectively:

$$\mathbf{S} = J_r\mathbf{F}_r^{-1}\boldsymbol{\sigma}\mathbf{F}_r^{-T} \tag{14}$$

$$\dot{\mathbf{E}}_r = \frac{1}{2}(\dot{\mathbf{F}}_r^T\mathbf{F}_r + \mathbf{F}_r^T\dot{\mathbf{F}}_r) \tag{15}$$

where $\dot{\mathbf{F}}_r$ is the rate of the deformation gradient.

By expressing the Eulerian strain rate in terms of the Green-Lagrange strain rate and substituting the eq. (6) into the eq. (14), we obtain:

$$\mathbf{S} = J_r\mathbf{F}_r^{-1}\left(\boldsymbol{\mathcal{D}} : (\mathbf{F}_r^{-T}\dot{\mathbf{E}}_r\mathbf{F}_r^{-1})\right)\mathbf{F}_r^{-T} - pJ_r\mathbf{C}_r^{-1} = \boldsymbol{\mathcal{D}}_r : \dot{\mathbf{E}}_r - pJ_r\mathbf{C}_r^{-1} \tag{16}$$

where $\boldsymbol{\mathcal{D}}_r$ is the 4th-order constitutive tensor in the reference configuration. This tensor can be calculated by applying a pull-back operation to the tensor defined in the current configuration Ω. Thus, we have in indicial notation:

$$(D_r)_{ijkl} = J_r\left(F_r^{-1}\right)_{ia}\left(F_r^{-1}\right)_{jb}\left(F_r^{-1}\right)_{kc}\left(F_r^{-1}\right)_{ld}D_{abcd} \tag{17}$$

3 Position-based finite element method

The procedure for obtaining the discrete finite element equation follows the procedure presented by Avancini et al. [14], which is based on the stationary energy principle taking the particle positions and nodal pressures as variational parameters.

The PFEM approach demands linear shape function for the approximation of both pressure and posistions. As a consequence, the Ladyzhenskaya-Babuska-Brezzi (LBB) conditions [28–30] are not satisfied, which can lead to spurious pressure solutions and numerical instability problems. To address this issue, the formulation employs the Pressure-Stabilized Petrov-Galerkin [31, 32], which constis of adding to the weak form, the residual of the momentum equation weighted by the gradient of the pressure test function multiplied by a stabilizing parameter.

The time integration is carried out through the generalized-α method, proposed by Chung and Hulbert [33], which is implicit and second-order accurate. It is unconditionally stable and allows for the control of numerical dissipation at high frequencies. The equilibrium is considered at an intermediate time $t_{n+\alpha}$, where the acceleration is interpolated at $t_{n+\alpha_m}$, while the velocity and positions are interpolated at $t_{n+\alpha_f}$. Velocity and acceleration at the current step t_{n+1} are firstly computed using Newmark approximations, and then used for the interpolation at $t_{n+\alpha}$. The parameters α_m and α_f, are determined as a function of the chosen spectral radius ρ_∞ (see Jansen et al. [34]), as shown in eq. (18) and eq. (19), allowing control over the dissipation at high frequencies. Additionally, the Newmark parameters β and γ are derived from α_m and α_f to ensure second order accuracy.

$$\alpha_m = \frac{1}{2}\left(\frac{3-\rho_\infty}{1+\rho_\infty}\right) \tag{18}$$

and

$$\alpha_f = \frac{1}{1+\rho_\infty}, \tag{19}$$

where $0 \leq \rho_\infty \leq 1$, resulting maximum high frequency dissipation for $\rho_\infty = 0$ and minimum dissipation for $\rho_\infty = 1$.

Ommiting the details of the discretization process, the fully discrete finite step problem is given by:

$$\begin{aligned}\frac{\partial \Pi_{n+\alpha}}{\partial(\mathbf{y}_a)_{n+\alpha}} = &\int_{\Omega_r} \rho_r N_a \ddot{\mathbf{y}}^h_{n+\alpha} d\Omega_r + \int_{\Omega_r} (\dot{\mathbf{E}}^h_r)_{n+\alpha} : (\boldsymbol{\mathcal{D}}^h_r)_{n+\alpha} : \frac{\partial (\mathbf{E}^h_r)_{n+\alpha}}{\partial(\mathbf{y}_a)_{n+\alpha}} d\Omega_r \\ &- \int_{\Omega_r} p^h_{n+1} \frac{\partial (J^h_r)_{n+\alpha}}{\partial(\mathbf{y}_a)_{n+\alpha}} d\Omega_r - \int_{\Omega_r} N_a \mathbf{b}_r d\Omega_r - \int_{\Gamma_r} N_a \mathbf{h}_r d\Gamma_r = \mathbf{0},\end{aligned} \tag{20}$$

$$\begin{aligned}\frac{\partial \Pi_{n+\alpha}}{\partial(p_a)_{n+1}} + (R_s)_{n+\alpha} = &- \int_{\Omega_r} N_a((J^h_r)_{n+\alpha} - 1) d\Omega_r + \int_{\Omega_r} \tau_{\mathrm{PSPG}} \frac{1}{\rho_r} (\mathbf{F}^h_r)^{-T}_{n+\alpha} \nabla_{\mathbf{x}_r} N_a \cdot \Big[\\ &\rho_r \ddot{\mathbf{y}}^h_{n+\alpha} - \nabla_{\mathbf{x}_r} \cdot \left((\mathbf{S}^h)_{n+\alpha} (\mathbf{F}^h_r)^T_{n+\alpha}\right) - \mathbf{b}_r \Big] d\Omega_r = 0.\end{aligned} \tag{21}$$

where Π is the energy functional, the index a represents the sum over element nodes (particles) a, the superscript h indicates an interpolated variable associated with the finite element discretization, N_a is the shape function relate to the node a, the index $n+\alpha$ represents the intermediate time, p^h_{n+1} is the pressure interpolated in the current time, τ_{PSPG} is the stabilization parameter, and R_s is the residual of the incompressibility condition.

The nonlinear system defined by eq. (20) and eq. (21) is solved iteratively using Newton-Raphson method, by recurrence of:

$$\begin{bmatrix} \frac{\partial}{\partial(\mathbf{y}_b)_{n+1}}\left(\frac{\partial \Pi_{n+\alpha}}{\partial(\mathbf{y}_a)_{n+\alpha}}\right) & \frac{\partial}{\partial(p_b)_{n+1}}\left(\frac{\partial \Pi_{n+\alpha}}{\partial(\mathbf{y}_a)_{n+\alpha}}\right) \\ \frac{\partial}{\partial(\mathbf{y}_b)_{n+1}}\left(\frac{\partial \Pi_{n+\alpha}}{\partial(p_a)_{n+1}} + (R_s)_{n+\alpha}\right) & \frac{\partial}{\partial(p_b)_{n+1}}(R_s)_{n+\alpha} \end{bmatrix}^k \cdot \begin{Bmatrix} \Delta \mathbf{y}_b \\ \Delta p_b \end{Bmatrix}^k = - \begin{Bmatrix} -\frac{\partial \Pi_{n+\alpha}}{\partial(\mathbf{y}_a)_{n+\alpha}} \\ \frac{\partial \Pi_{n+\alpha}}{\partial(p_a)_{n+1}} + (R_s)_{n+\alpha} \end{Bmatrix}^k . \tag{22}$$

where the superscript k denotes the iteration number, $\Delta \mathbf{y}_b$ and Δp_b are the position and pressure increments of a node b, and right side vectors are the residual vectors of node a. The criterion for solution convergence is based on the norm of the increments in position and pressure, which must be smaller than a predefined tolerance.

4 Particle finite element method

This work employs the classical Particle Finite Element Method (PFEM) as outlined by Idelsohn et al. [10]. The procedure begins by discretizing the fluid domain using particles. Delaunay triangulation is then applied to generate a convex mesh from these particles, utilizing the open-source library Tetgen (see Si [35]) for 3D analyses.

Subsequently, the α-shape method, as described by Edelsbrunner and Mücke [36], removes excessively distorted or large elements with $r_e > \alpha_e h_e$, where r_e is the element's circumscribed radius, α_e is a user-defined parameter, and h_e is the element's characteristic length. This last procedure defines the boundary of the domain.

The discretized equations (eq. (20) and eq. (21)) are solved to determine the configuration at time $t + 1$. If elements are highly distorted, remeshing is performed to regenerate the mesh while preserving nodal values. To maintain mesh quality, nodes are relocated if an element's edge length is below 0.6 times the characteristic length, or if the cosine of the angles between tetrahedron faces exceeds 0.99.

5 Numerical study

The proposed methodology was validated using experimental and numerical results from a slump-flow test of fresh concrete, from the studies by Cremonesi et al. [18] and Franci and Zhang [17]. In this test, a truncated cone is filled with fresh concrete. Then, it lifted, and the concrete flow starts onto a base plate, by the action of gravity. The evolution on time of the spreading diameter was obtained with a 4c-rheometer (see Thrane et al. [37]).

The geometry of the simulation consists of a three-dimensional concrete volume with a truncated cone shape, having a diameter of 0.1 m at the top, 0.2 m at the bottom, and a height of 0.3 m. This volume rests on a base with a diameter of 0.7 m. Regarding the boundary conditions, there is no slip between the concrete and the base, and the base is fixed in all directions. An external body force, equals to $\rho_r g$, is applied, with gravity being $9.81 m/s^2$ in the vertical direction of the cone. The outer surfaces of the concrete are free to move. Additionally, the material properties are $\rho = 2200.0$ kg/m^3, $\mu_p = 255.0$ Pa.s, $\tau_0 = 32.0$ Pa.

Regarding the numerical aspects, a spectral radius of 0.8, an α-shape parameter of 1.35, a time step of $0.005s$, and a total of 8000 steps, totaling $40s$ of simulation, were set. The simulation mesh consists of 60042 tetrahedral elements, compared to the 54464 elements in the mesh presented by Franci and Zhang [17]. Figure 1 compares the velocity contours over the deformed configuration at $t = 5.0s$ from Franci and Zhang [17] and the present work, showing qualitative agreement. Figure 2 shows the time evolution of the spreading diameter from numerical and experimental results. The numerical results align well with the experimental data and improve upon those by Franci and Zhang [17], demonstrating the effectiveness of the proposed methodology.

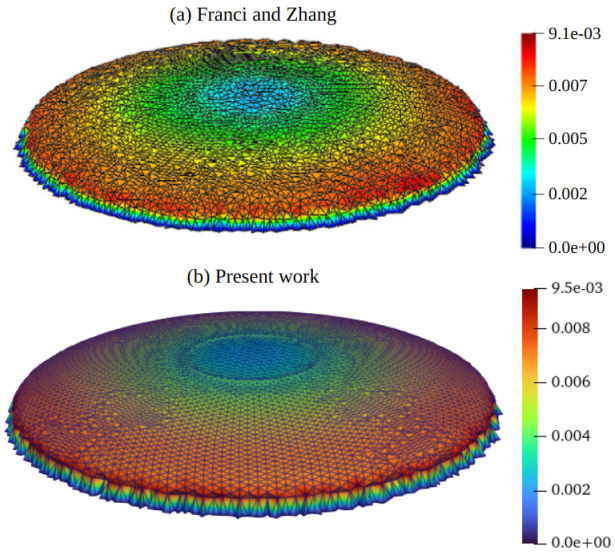

Figure 1. Comparison of velocity contours plotted over the deformed configuration at $t = 5.0s$ by Franci and Zhang [17] and the present work; units are in m/s

6 Conclusions

The methodology to extend the application of the particle-position-based PFEM formulation to incompressible non-Newtonian fluids was presented. The implementation was tested using a numerical example of a slump-flow test of fresh concrete, showing good agreement with experimental data and an improvement over previous numerical results. Further investigation is needed to assess the robustness and accuracy of the methodology in other examples. The authors are also interested in implementing other viscoplastic models, such as the Herschel-Bulkley model, which more accurately represent the behavior of fresh concrete.

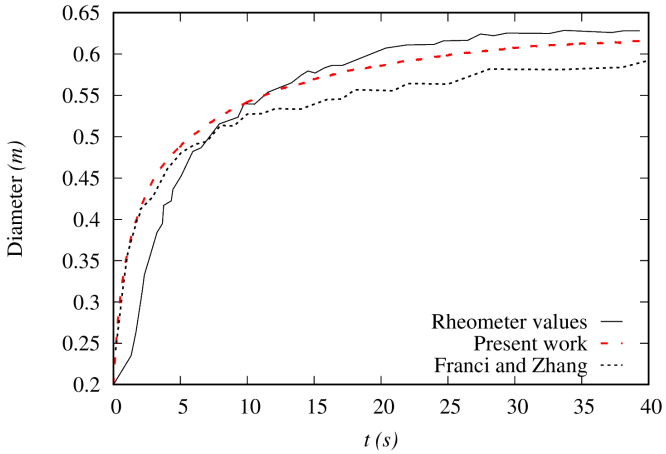

Figure 2. Evolution on time of the spreading diameter from numerical and experimental results

Acknowledgements. This study was financed in part by the Coordenação de Aperfeiçoamento de Pessoal de Nível Superior - Brasil (CAPES) - Finance Code 001, and by Brazilian National Council for Research and Technological Development (CNPq) - grant - 314045/2023-6. The authors would like to thank them for the financial support given to this research. The authors are also grateful for the infrastructure of the Department of Structures SET/EESC and the University of Sao Paulo.

Authorship statement. The authors hereby confirm that they are the sole liable persons responsible for the authorship of this work, and that all material that has been herein included as part of the present paper is either the property (and authorship) of the authors, or has the permission of the owners to be included here.

References

[1] J. E. Welch, F. H. Harlow, J. P. Shannon, and B. J. Daly. The mac method-a computing technique for solving viscous, incompressible, transient fluid-flow problems involving free surfaces, 1965.
[2] W. F. Noh and P. Woodward. Slic (simple line interface calculation). In van de A. I. Vooren and P. J. Zandbergen, eds, *Proceedings of the Fifth International Conference on Numerical Methods in Fluid Dynamics June 28 – July 2, 1976 Twente University, Enschede*, pp. 330–340, Berlin, Heidelberg. Springer Berlin Heidelberg, 1976.
[3] C. W. Hirt and B. D. Nichols. Volume of fluid (VOF) method for the dynamics of free boundaries. *Journal of Computational Physics*, vol. 39, n. 1, pp. 201–225, 1981.
[4] S. Osher and J. A. Sethian. Fronts Propagating with Curvature-Dependent Speed: Algorithms Based on Hamilton-Jacobi Formulations. *Journal of Computational Physics*, vol. 79, pp. 12–49, 1988.
[5] C. W. Hirt, A. A. Amsden, and J. L. Cook. An arbitrary Lagrangian-Eulerian computing method for all flow speeds. *Journal of Computational Physics*, vol. 14, n. 3, pp. 227–253, 1974.
[6] G. Avancini and R. A. Sanches. A total Lagrangian position-based finite element formulation for free-surface incompressible flows. *Finite Elements in Analysis and Design*, vol. 169, pp. 103348, 2020.
[7] P. A. Cundall and O. D. Strack. A discrete numerical model for granular assemblies. *Geotechnique*, vol. 29, n. 1, pp. 47–65, 1979.
[8] R. A. Gingold and J. J. Monaghan. Smoothed particle hydrodynamics: theory and application to non-spherical stars. *Monthly Notices of the Royal Astronomical Society*, vol. 181, n. 3, pp. 375–389, 1977.
[9] S. Koshizuka and Y. Oka. Moving-Particle Semi-Implicit Method for Fragmentation of Incompressible Fluid. *Nuclear Science and Engineering*, vol. 123, n. 3, pp. 421–434, 1996.
[10] S. R. Idelsohn, E. Onate, and F. Del Pin. The particle finite element method: a powerful tool to solve incompressible flows with free-surfaces and breaking waves. *International Journal for Numerical Methods in Engineering*, vol. 61, n. 7, pp. 964–989, 2004.
[11] M. Cremonesi, A. Franci, S. Idelsohn, and E. Oñate. A State of the Art Review of the Particle Finite Element Method (PFEM). *Archives of Computational Methods in Engineering*, vol. 27, n. 5, pp. 1709–1735, 2020.
[12] H. B. Coda. An exact fem geometric non-linear analysis of frames based on position description. In *International Congress of Mechanical Engineering*. ABCM, 2003.
[13] J. Bonet, R. D. Wood, J. Mahaney, and P. Heywood. Finite element analysis of air supported membrane structures. *Computer Methods in Applied Mechanics and Engineering*, vol. 190, n. 5-7, pp. 579–595, 2000.

[14] G. Avancini, A. Franci, S. Idelsohn, and R. A. Sanches. A particle-position-based finite element formulation for free-surface flows with topological changes. *Computer Methods in Applied Mechanics and Engineering*, vol. 429, pp. 117118, 2024.
[15] J. Reinold, V. N. Nerella, V. Mechtcherine, and G. Meschke. Extrusion process simulation and layer shape prediction during 3D-concrete-printing using the Particle Finite Element Method. *Automation in Construction*, vol. 136, 2022.
[16] J. Reinold and G. Meschke. A mixed u–p edge-based smoothed particle finite element formulation for viscous flow simulations. *Computational Mechanics*, vol. 69, n. 4, pp. 891–910, 2022.
[17] A. Franci and X. Zhang. 3D numerical simulation of free-surface Bingham fluids interacting with structures using the PFEM. *Journal of Non-Newtonian Fluid Mechanics*, vol. 259, pp. 1–15, 2018.
[18] M. Cremonesi, L. Ferrara, A. Frangi, and U. Perego. Simulation of the flow of fresh cement suspensions by a Lagrangian finite element approach. *Journal of Non-Newtonian Fluid Mechanics*, vol. 165, n. 23-24, pp. 1555–1563, 2010.
[19] Y. Li, J. Mu, Z. Wang, Y. Liu, and H. Du. Numerical simulation on slump test of fresh concrete based on lattice Boltzmann method. *Cement and Concrete Composites*, vol. 122, pp. 104136, 2021.
[20] T. Tran-Duc, T. Ho, and N. Thamwattana. A smoothed particle hydrodynamics study on effect of coarse aggregate on self-compacting concrete flows. *International Journal of Mechanical Sciences*, vol. 190, 2021.
[21] M. S. Abo Dhaheer, S. Kulasegaram, and B. L. Karihaloo. Simulation of self-compacting concrete flow in the J-ring test using smoothed particle hydrodynamics (SPH). *Cement and Concrete Research*, vol. 89, pp. 27–34, 2016.
[22] H. Lashkarbolouk, M. R. Chamani, A. M. Halabian, and A. R. Pishehvar. Viscosity evaluation of SCC based on flowsimulation in the L-box test. *Magazine of Concrete Research*, vol. 65, n. 6, pp. 365–376, 2013.
[23] S. Jiang, Z. He, Y. Zhou, X. Xiao, G. Cao, and Z. Tong. Numerical simulation research on suction process of concrete pumping system based on CFD method. *Powder Technology*, vol. 409, pp. 117787, 2022.
[24] J. Mu, Y. Li, C. Jin, and Y. Liu. Simulation of U-box test for fresh self-compacting concrete based on lattice Boltzmann method. *Construction and Building Materials*, vol. 351, pp. 128922, 2022.
[25] D. Feys, J. E. Wallevik, A. Yahia, K. H. Khayat, and O. H. Wallevik. Extension of the Reiner-Riwlin equation to determine modified Bingham parameters measured in coaxial cylinders rheometers. *Materials and Structures/Materiaux et Constructions*, vol. 46, n. 1-2, pp. 289–311, 2013.
[26] M. Hosseinpoor, K. H. Khayat, and A. Yahia. Numerical simulation of self-consolidating concrete flow as a heterogeneous material in L-Box set-up: coupled effect of reinforcing bars and aggregate content on flow characteristics. *Materials and Structures/Materiaux et Constructions*, vol. 50, n. 2, pp. 1–15, 2017.
[27] T. C. Papanastasiou. Flows of Materials with Yield. *Journal of Rheology*, vol. 31, n. 5, pp. 385–404, 1987.
[28] I. Babuška. The finite element method with Lagrangian multipliers. *Numerische Mathematik*, vol. 20, n. 3, pp. 179–192, 1973.
[29] Brezzi, F. On the existence, uniqueness and approximation of saddle-point problems arising from lagrangian multipliers. *R.A.I.R.O. Analyse Numérique*, vol. 8, pp. 129–151, 1974.
[30] I. Babuška and R. Narasimhan. The babuška-brezzi condition and the patch test: an example. *Computer Methods in Applied Mechanics and Engineering*, vol. 140, n. 1, pp. 183–199, 1997.
[31] T. E. Tezduyar. Stabilized finite element formulations for incompressible flow computations. *Advances in applied mechanics*, vol. 28, pp. 1–44, 1991.
[32] T. Tezduyar, S. Mittal, S. Ray, and R. Shih. Incompressible flow computations with stabilized bilinear and linear equal-order-interpolation velocity-pressure elements. *Computer Methods in Applied Mechanics and Engineering*, vol. 95, n. 2, pp. 221–242, 1992.
[33] J. Chung and G. M. Hulbert. A Time Integration Algorithm for Structural Dynamics With Improved Numerical Dissipation: The Generalized-α Method. *Journal of Applied Mechanics*, vol. 60, n. 2, pp. 371–375, 1993.
[34] K. E. Jansen, C. H. Whiting, and G. M. Hulbert. A generalized-α method for integrating the filtered navier–stokes equations with a stabilized finite element method. *Computer Methods in Applied Mechanics and Engineering*, vol. 190, n. 3, pp. 305–319, 2000.
[35] H. Si. Tetgen, a delaunay-based quality tetrahedral mesh generator. *ACM Trans. Math. Softw.*, vol. 41, n. 2, 2015.
[36] H. Edelsbrunner and E. P. Mücke. Three-dimensional alpha shapes. *ACM Transactions on Graphics (TOG)*, vol. 13, n. 1, pp. 43–72, 1994.
[37] L. N. Thrane, C. Pade, and C. V. Nielsen. Determination of rheology of self-consolidating concrete using the 4c-rheometer and how to make use of the results. *Journal of Astm International*, vol. 7, pp. 1–10, 2010.